HHS Public Access

Author manuscript

Science. Author manuscript; available in PMC 2024 January 12.

Published in final edited form as:

Science. 2023 December 22; 382(6677): 1404–1411. doi:10.1126/science.adi9926.

Rab29-dependent asymmetrical activation of leucine-rich repeat kinase 2

Hanwen Zhu[1,†], **Francesca Tonelli**[2,3,†], **Martin Turk**[4], **Alan Prescott**[2], **Dario R. Alessi**[2,3], **Ji Sun**[1,*]

[1]Department of Structural Biology, St. Jude Children's Research Hospital, Memphis, TN 38105, USA

[2]MRC Protein Phosphorylation and Ubiquitylation Unit, School of Life Sciences, University of Dundee, Dundee DD1 5EH, UK

[3]Aligning Science Across Parkinson's (ASAP) Collaborative Research Network, Chevy Chase, MD, USA

[4]Cryo-EM and Tomography Center, St. Jude Children's Research Hospital, Memphis, TN 38105, USA

Abstract

Gain-of-function mutations in *LRRK2*, which encodes the leucine-rich repeat kinase 2 (LRRK2), are the most common genetic cause of late-onset Parkinson's Disease. LRRK2 is recruited to membrane organelles and activated by Rab29, a Rab guanosine triphosphatase encoded in the *PARK16* locus. We present cryo–electron microscopy structures of Rab29–LRRK2 complexes in three oligomeric states, providing key snapshots during LRRK2 recruitment and activation. Rab29 induces an unexpected tetrameric assembly of LRRK2, formed by two kinase-active central protomers and two kinase-inactive peripheral protomers. The central protomers resemble the active-like state trapped by the type I kinase inhibitor DNL201, a compound that underwent a phase 1 clinical trial. Our work reveals the structural mechanism of LRRK2 spatial regulation and provides insights into LRRK2 inhibitor design for Parkinson's disease treatment.

*Corresponding author. ji.sun@stjude.org.
†These authors contributed equally to this work.

Author contributions: H.Z. and J.S. designed the project. H.Z. performed sample preparation, biochemical analysis, and structural determination. F.T. designed, performed, and analyzed the cellular assays. F.T. and D.R.A. interpreted the activity assays. A.P. acquired and quantified the confocal microscopy images blindly. H.Z. optimized and performed the kinase inhibition assay. M.T. performed the 2D classification cross-correlation analysis. All authors were involved in data analysis. H.Z. and J.S. wrote the manuscript with input from all authors.

Competing interests: The authors declare that they have no competing interests.

Supplementary Materials
science.org/doi/10.1126/science.adi9926
Materials and Methods
Figs. S1 to S11
Table S1
Movies S1 and S2
References (60–72)
MDAR Reproducibility Checklist

Parkinson's disease (PD) is the second most prevalent neurodegenerative disorder, affecting 1 to 2% of the population over the age of 65 (1). Mutations in the *LRRK2* gene, which encodes the leucine-rich repeat kinase 2 (LRRK2) protein, are among the most frequent genetic causes of late-onset PD and account for ~5% of familial and ~1% of sporadic cases (2–4). More than 250 mutations in *LRRK2* have been identified, and ~100 were biochemically characterized (5–7). Most LRRK2-related PD mutations, such as G2019S (Gly^{2019}→Ser), have increased kinase activity. Therefore, LRRK2 inhibitors are of great interest to researchers in PD treatment (2).

Much effort has been directed at exploring the structure-function relationship in LRRK2 to gain a mechanistic understanding and to guide rational drug discovery (8). Previous work revealed high-resolution structures of inactive LRRK2 (9, 10), whereas our understanding of LRRK2 activation is limited to microtubule-associated LRRK2 structures of disease mutations at mediate and low resolutions (11, 12) or molecular dynamics (MD) simulations in combination with hydrogen-deuterium exchange mass spectrometry (HDX-MS) analyses (13–16). Furthermore, LRRK2 activation in both physiological and pathogenic conditions is tightly associated with membrane recruitment and Rab guanosine triphosphatases (GTPases) (17–19), the molecular basis of which remains enigmatic.

This study aimed to explore the kinase activation mechanism of LRRK2 that is induced by Rab29, a membrane-anchored Rab GTPase. Rab GTPases are master regulators of intracellular-vesicle trafficking, whose disruption is a hallmark of PD pathogenesis (20). Rab29, encoded in the *PARK16* locus and associated with late-onset PD, is believed to function in the same pathway as LRRK2. Although mouse genetic data suggest that alternative activation mechanisms of LRRK2 exist (21), physiological connections between Rab29 and LRRK2 are supported by human and *Caenorhabditis elegans* genetic data, similar mouse knockout histological phenotypes, cellular colocalization, and physical interactions (22–27). Moreover, Rab29, but not its close homologs Rab32 or Rab38, stimulates LRRK2 kinase activity by monitoring S1292 autophosphorylation (28), suggesting that Rab29 does more than membrane recruitment to stimulate LRRK2 activity.

Structural determination of Rab29–LRRK2 complexes

To structurally characterize the Rab29–LRRK2 interaction, we first reconstituted a stable complex in vitro. Previous studies have suggested an emerging "Rab29–LRRK2–Rabs" cascade for LRRK2 signaling (Fig. 1A) (19, 29), in which GTP-bound Rab29 (Rab29•GTP) facilitates LRRK2 membrane recruitment and activation, then activated LRRK2 phosphorylates Rab GTPases, including Rab29 itself. Phosphorylated Rab29, which was reported not to activate LRRK2, could potentially serve as negative feedback (28). We thus introduced three point mutations (Q67L, T71A, and S72A) to Rab29 ($Rab29_{EM}$) to maximize the opportunity of capturing the active Rab29•GTP–LRRK2 complex (where Q is glutamine, L is leucine, T is threonine, A is alanine, and S is serine). T71A and S72A prevent Rab29 phosphorylation, and Q67L abolishes GTPase activity and enhances the interaction between Rab29 and LRRK2 (26). Although Q67L also diminishes the membrane localization of Rab29 in cells (26), we reasoned that the interaction between Rab29 and

LRRK2 is independent of membrane environment or composition (30) and should not be affected in vitro by this mutation. Indeed, glutathione *S*-transferase (GST) pulldown assays validated the $Rab29_{EM}$–LRRK2 interaction and complex formation (fig. S2G).

We determined cryo–electron microscopy (cryo-EM) structures of the Rab29–LRRK2 complex, reconstituted by mixing LRRK2, $Rab29_{EM}$, GTP analog (GppNHp), adenosine triphosphate (ATP), and Mg^{2+}. The final cryo-EM reconstruction resulted in Rab29–LRRK2 structures of three distinct oligomeric assemblies (Fig. 1, B and C; fig. S1; and table S1): Rab29–LRRK2 monomer with one LRRK2 and one Rab29; Rab29–LRRK2 dimer with two LRRK2 and two Rab29; and Rab29–LRRK2 tetramer with four LRRK2 and two visible Rab29 (Fig. 1, B and C). Focused three-dimensional (3D) refinement improved the cryo-EM density surrounding the Rab29–LRRK2 interface (fig. S1A), and C2 symmetry was imposed for Rab29–LRRK2 dimer and tetramer during data analysis (fig. S1A).

Rab29-dependent recruitment of LRRK2

In the Rab29–LRRK2 monomer, LRRK2 is almost identical to the inactive LRRK2-alone structure (10) (fig. S2A). Rab29 binds to the N-terminal armadillo repeat (ARM) domain of LRRK2, burying a surface area of ~800 $Å^2$ (Fig. 2A), and adopts a GTP-bound Switch I closed configuration often observed in GTP-bound small GTPases (fig. S2, B to E). Docking of the GDP-bound Rab29 structure (25) into the cryo-EM density shows obvious steric clashes with LRRK2 (fig. S2F), explaining why the GTP-bound state promotes Rab29-dependent recruitment of LRRK2 (24, 25, 27, 28, 30, 31).

The Rab29–LRRK2 interface is formed by the ARM9-10 of LRRK2 and the Switch I-Interswitch-Switch II surface and CDR1 (32) of Rab29 (fig. S2E). The interaction conforms with a general Rab-effector recognition mode, in which effectors associate with the GTP-bound form of Rabs through the Switch I-Interswitch-Switch II surface (32). Sequence alignment of Rab GTPases, including the Rab32 subfamily (Rab29, Rab32, and Rab38) and several LRRK2 substrates, revealed that key residues in the Rab29–LRRK2 interface were conserved among the Rab32 subfamily (fig. S2H). Single mutations at the center of the interface (Rab29 D43A or W62A) were sufficient to abolish the interaction, whereas Rab29 L7Q or L76M substitutions at the edge of the interface had moderate or little impact (fig. S2G). The surfaces of Rab29 and Rab10 predicted to interact with LRRK2 had almost identical interface residues, which is consistent with previous work suggesting that Rab10 interacts with LRRK2 at the Rab29 site (33). Rab5A, 5B, and 5C, which can be phosphorylated by LRRK2 (34), contain an alanine in the position corresponding to Asp^{43} in Rab29 (fig. S2H).

Consistent with the pulldown-assay results, confocal microscopy revealed that Rab29 D43A or W62A mutations diminished the membrane recruitment of LRRK2, whereas Rab29 L7Q or L76M substitutions had moderate or little disruptive effects (Fig. 2B and fig. S3A). Similarly, LRRK2 mutations (R399E and L403E) at the center of the Rab29–LRRK2 interface significantly reduced the Rab29-dependent membrane recruitment, whereas a mutation at the periphery of the interface (M402A) had a moderate impact (Fig. 2C and fig. S3B). We also assessed the effect of interface mutations on LRRK2 kinase activity

in cells by monitoring the phosphorylation status of Rab10-Thr^{73}, Rab29-Thr^{71}, and LRRK2-Ser^{1292} (28). In agreement with the pulldown and membrane-localization results, mutations at the center of the interface on either the Rab29 (Fig. 2D and fig. S3, C and E) or LRRK2 side (Fig. 2E and fig. S3D) abolished the Rab29-stimulated kinase activity, whereas mutations at the periphery had only a minor impact. These data confirmed the observed Rab29–LRRK2 interface and suggested the importance of membrane recruitment for LRRK2 activation. All mutations introduced to the Rab29–LRRK2 interface had minor impacts on the basal activity of LRRK2 on Rab10 and Ser^{1292}, supporting the view that the observed interface is important for LRRK2 recruitment but probably not for substrate recognition.

In the Rab29–LRRK2 dimer assembly, each LRRK2 protomer binds a single Rab29 molecule at the ARM9-10 interface (Fig. 1B). In this X-shaped complex, LRRK2 protomers adopt the same inactive conformation observed in the Rab29–LRRK2 monomer and the LRRK2-alone structure (fig. S4) (10). The two LRRK2 protomers interact via their COR-B domains, in a way that is similar to what we described for the LRRK2 homodimer (fig. S4B) (10). The observation of LRRK2 dimers both in the presence and absence of Rab29 suggests that COR-B–mediated dimerization of LRRK2 could occur under physiological settings.

A tetrameric assembly of LRRK2

We captured the Rab29–LRRK2 complex in an unexpected tetrameric assembly and determined its structure to an overall resolution of 3.5 Å (fig. S1 and table S1). With a ~205 Å by 260 Å by 150 Å dimension (Fig. 1, B and C), the Rab29–LRRK2 tetramer is an assembly with a twofold rather than fourfold symmetry, featuring two types of LRRK2 protomers: LRRK2^{peri} (peripheral) and LRRK2^{cent} (central) (Fig. 1, B and C, and Fig. 3A). We were able to resolve and model near full-length LRRK2^{peri} and associated Rab29^{peri}. By contrast, LRRK2^{cent} protomers have flexible LRR, ankyrin repeat (ANK), and ARM domains, and neither those domains nor the associated Rab29^{cent} molecules could be resolved (Fig. 3A and fig. S5, A to C). By contrast, the catalytic halves of LRRK2^{cent}, including ROC, COR, KIN, and WD40 domains (ROC, Ras of complex proteins; COR, C-terminal of ROC; KIN, kinase), were rigid and could be refined to an overall resolution of 3.2 Å with focused refinement (fig. S1A).

The LRRK2^{peri}–LRRK2^{cent} interaction within each asymmetric unit is mediated by the COR-B domains (fig. S5, C and D), and the COR-B–COR-B interface is similar to that seen in LRRK2 homodimers or Rab29–LRRK2 dimers, with a subtle rotational motion (fig. S5D). In addition, LRRK2^{peri} directly interacts with LRRK2^{cent} from the other asymmetric unit (Fig. 3, A to C), with regions near the LRRK2^{peri} ARM–ANK boundary packing against the LRRK2^{cent} WD40 domain and the LRRK2^{peri} ARM domain associated with the LRRK2^{cent} ROC domain. The two LRRK2^{cent} protomers pack in a “head-to-tail” mode through WD40–KIN interfaces (Fig. 3, A and D). The flexible N-terminal part of LRRK2^{cent} might also interact with the Rab29^{peri} and the ARM domain of LRRK2^{peri}, but the low local resolution of the cryo-EM map prevents further interpretation (fig. S5A).

The catalytic halves of LRRK2^{cent} and LRRK2^{peri} show substantial conformational differences (Fig. 3E and movie S1). Upon aligning the COR-B domain, KIN and WD40 are displaced about 40° toward the COR-A and ROC domains in LRRK2^{cent} (fig. S5E). This conformational rearrangement closes a central cavity shaped by the ROC, COR, and KIN domains (Fig. 3E). In this conformation, COR-B, ROC-COR-A, KIN N-lobe, and KIN C-lobe-WD40 appear to move as rigid bodies (fig. S5F). Repositioning of KIN C-lobe-WD40 in LRRK2^{cent} disrupts the connection between the WD40 and ARM-ANK-LRR domains in the inactive state, which was stabilized by the scaffolding hinge helix and C-terminal helix (fig. S5, G and H) (10). Additionally, the KIN C-lobe would clash into the LRR domain (fig. S5I), contributing to the displacement and flexibility of the ARM-ANK-LRR domains in LRRK2^{cent} protomers (fig. S5A).

LRRK2^{cent} has an active kinase domain

The KIN domain of LRRK2^{cent} has structural features of an active kinase. The LRR domain that shields the KIN domain in the inactive conformation (10) is flexible in LRRK2^{cent}, leaving the KIN domain accessible to substrates from the membrane side (fig. S5, A and B). Critically, the LRRK2^{cent} KIN domain adopts a closed conformation (Fig. 4A), with the αC helix positioned toward the active site and the “DYG motif’ flipped in. Lys^{1906} and Glu^{1920} form a salt bridge, an interaction blocked by Tyr^{2018} in the inactive conformation (Fig. 4, B and C). There is a well-defined cryo-EM density for ATP in the active site, and the distance between Asp^{2017} and ATP shortens to 3.8 Å (from 13.8 Å in the inactive state) (Fig. 4, A and C), permitting ATP hydrolysis in the presence of substrates. The regulatory spine (R-spine), formed by Leu^{1935}, Leu^{1924}, Tyr^{2018}, and Tyr^{1992} becomes continuous (Fig. 4D). Docking of the LRRK2^{cent} model into the 14-Å in situ cryo–electron tomography (cryo-ET) map of microtubule-bound LRRK2 (Fig. 4E), which was proposed to represent an active conformation (11), reveals close correspondence, supporting our conclusion that the LRRK2^{cent} KIN domain is in an active conformation.

We next examined the interdomain interactions that stabilize the active conformation of the LRRK2^{cent} KIN domain. The activation loop of the KIN domain (35) dips into the open pocket between COR-A and COR-B (Fig. 4F). We hypothesized that this interdomain interaction stabilizes the closed conformation of the KIN domain and would thus be crucial for LRRK2 kinase activity. Indeed, single point mutations at the KIN–COR interface (P1588A, N1710A, and W1791A) reduced the LRRK2 kinase activity induced by Rab29 (Fig. 4G and fig. S6). LRRK2-W1791A almost completely abolished LRRK2 activity in the absence of Rab29, indicating that the observed interactions (Fig. 4F) are also critical for the basal activity of LRRK2 (Fig. 4G and fig. S6C). Therefore, blocking the COR–KIN interaction could be a potential strategy to inhibit LRRK2 allosterically.

Compared with the inactive state, the KIN N-lobe rotates slightly toward the COR-B domain in LRRK2^{cent}, leading to more-extensive interactions between the αC helix of the KIN domain and the docking (Dk) helix of the COR-B domain (Fig. 4F). These observations are consistent with previous HDX-MS and MD simulation studies that indicated an altered interface between the COR-B Dk helix and the KIN αC helix and the stabilization of a nearby COR-B loop (residues 1721 to 1725) upon binding of type I inhibitors (fig. S5J) (15).

The ROC domain is displaced relative to the COR-B domain upon LRRK2 activation (fig. S5K). COR-B structurally bridges the catalytic ROC and KIN domains, and GTP binding in the former modulates the kinase activity of the latter (36–39). The movement of the ROC domain relative to the COR-B domain upon activation involves a “seesaw-like” motion of the ROC αC helix, with Tyr^{1699} as the pivot point (fig. S5K and movie S2). Our structural observations indicate that conformational coupling between the ROC and COR-B domains is vital for LRRK2 activity by contributing to the crosstalk between GTPase and kinase activities (10).

We then determined the cryo-EM structure of $LRRK2^{RCKW}$ (RCKW: ROC-COR-KIN-WD40) in complex with DNL201/GNE-0877, a compound reported to be safe and well tolerated in a phase 1 clinical trial (40) (Fig. 5A and fig. S7, A to H). $LRRK2^{RCKW}$ is used to simplify the structure determination caused by the flexibility of the N-terminal domains. DNL201 is a type I kinase inhibitor that fixes the LRRK2 kinase domain in an active-like conformation, as judged by the compound’s ability to induce dephosphorylation of Ser^{935} (40, 41). The well-resolved kinase domain structure revealed a binding site for DNL201 within LRRK2 at the ATP-binding pocket (Fig. 5B and fig. S7, F to H). In the $LRRK2^{cent}$ and $LRRK2^{RCKW}$–DNL201 structures, KIN domains adopted a highly similar structure [root mean square deviation (RMSD), 0.7 Å] (Fig. 5C), further supporting the active conformation of $LRRK2^{cent}$ KIN domain.

Comparing the active conformations of $LRRK2^{cent}$ and $LRRK2^{RCKW}$–DNL201, we observed several common features. The αC helix, activation loop, APE-αF, and αH-αI linkers from the KIN domain are the major contributors for interactions with COR, and the interface between the KIN and COR domains are almost identical (Fig. 5D) despite a small displacement of COR domains (Fig. 5C). The seesaw motion between the COR-B and ROC domains is also observed, as seen by the Tyr^{1699} side-chain flipping (fig. S8A). However, these activation features are different from or were not observed in the previous microtubule-based LRRK2 model (PDB 6XR4) (fig. S8B) (11). Additionally, there are global differences between Rab29-dependent and microtubule-based activation of LRRK2 because the Rab29–LRRK2 tetramer contains asymmetric dimers and microtubule-based LRRK2 oligomers are symmetric (fig. S8, C and D).

The conformational changes revealed by comparing active $LRRK2^{cent}$ or active-like LRRK2–DNL201 with inactive LRRK2 align very well with previous HDX-MS data (13–16). Overall, the active conformation has a more compact arrangement; the αC helix, activation loop, APE-αF loop of the KIN domain (Fig. 4F and Fig. 5D), and C-terminal part of COR-B helix (residues 1788 to 1797) showed lower deuterium exchange (14, 15), owing to the closure of the central cavity upon activation (Fig. 3E). The only exception was the C-terminal half of the αC helix of ROC domain (residues 1426 to 1449), which became more accessible and showed increased deuterium exchange because of the seesaw motion (fig. S5K).

Rab29–LRRK2 tetramer and Rab29-dependent activation

As the Rab29–LRRK2 tetramer has two protomers in active kinase conformation, we hypothesized that the tetrameric assembly could explain the increased Rab29-induced LRRK2 Ser^{1292} autophosphorylation (28). To test the hypothesis, we first verified that the tetramer state was not caused by the Rab29 Q67L mutation, which disrupts Rab29 membrane localization and impacts the Rab29-dependent LRRK2 activation in cells (23, 27). Thus, we characterized the Rab29 T71A/S72A–LRRK2 complex because Rab29 T71A/S72A has minimal impacts on LRRK2 cellular localization or kinase activity (fig. S9, A to D) (28). Our cryo-EM analysis showed that Rab29 T71A/S72A–LRRK2 forms tetramers during 2D classification performed with cross-correlation (fig. S9E), although there was a lower ratio of tetramer particles than with $Rab29_{EM}$–LRRK2, likely because of a lower percentage of GTP-bound Rab29.

We then compared Rab29–LRRK2 and Rab32–LRRK2 complexes to dissect the role of LRRK2 tetramerization in kinase activation. Rab32, a close homolog of Rab29 (~56% sequence identity and ~70% similarity) can mediate LRRK2 membrane recruitment (31) but does not support LRRK2 activation in human embryonic kidney 293 (HEK293) cells, as indicated by low Ser^{1292} autophosphorylation levels (28) and by a higher level of Ser^{935} phosphorylation (Fig. 6, A and B), which is associated with inactive LRRK2 (41). We determined the cryo-EM structure of Rab32–LRRK2 complexes (fig. S10, A to C). Rab32 interacts with LRRK2 through an interface that is almost identical to that used by Rab29 (fig. S10, D and E), but the Rab32–LRRK2 complex was captured in two oligomerization states: Rab32–LRRK2 monomer and Rab32–LRRK2 dimer (Fig. 6C). Furthermore, reprocessing of our previous LRRK2-alone dataset (10) showed no LRRK2 tetrameric assembly (Fig. 6D and fig. S10F). Therefore, we conclude that the Rab29–LRRK2 tetramer is associated with the Rab29-dependent activation of Ser^{1292} autophosphorylation.

In contrast to our results for Ser^{1292} autophosphorylation, we found that phosphorylation of Rab10 by LRRK2 is stimulated by both Rab29 and Rab32 (Fig. 6B), suggesting that membrane recruitment of LRRK2 is sufficient to activate Rab10 phosphorylation without a requirement for tetramerization. Rab10 phosphorylation and Ser^{1292} autophosphorylation are thus independent molecular events during LRRK2 signaling (42, 43). Endogenous Rab38 was also reported to increase Rab10 phosphorylation but not Ser^{1292} autophosphorylation in melanocytes (44). Therefore, we predict that Rab38 should mediate LRRK2 membrane recruitment but not the tetramerization of LRRK2.

Discussion

In this study, we have presented Rab29–LRRK2 structures in both active and inactive states, which allowed us to analyze PD mutations in the context of kinase activation. Gain-of-function mutations at six sites—G2019S, I2020T, Y1699C, N1437H, R1441C/G/H, and S1761R (fig. S11A)—have been proposed to be high risk and PD-causing (45). Our previous structure of LRRK2 bearing the G2019S substitution showed little difference from the wild-type (WT) LRRK2 in the inactive state (10). However, this mutation could induce additional

interactions with Glu^{1920} and stabilize the critical Lys^{1906}-Glu^{1920} salt bridge in the active conformation (fig. S11C). Ile^{2020} moves from a hydrophobic to a hydrophilic environment upon LRRK2 activation (fig. S11B), and the I2020T mutation would destabilize the inactive conformation and favor the active conformation. Tyr^{1699}, Asn^{1437}, and Arg^{1441} are at the interface between the αC helix of ROC and the COR-B domain, where a seesaw-like motion of the ROC-αC helix occurs upon LRRK2 activation (fig. S11D, fig. S5K, and movie S2). Asn^{1437} and Arg^{1441} are located at one side of the seesaw and anchor the C-terminal part on the αC helix of ROC to the surface of the COR-B domain in the inactive state (fig. S11D). Therefore, mutations of Asn^{1437} and Arg^{1441} should weaken the anchoring effect, shifting the balance of the seesaw toward the N-terminal of the ROC αC helix, hence promoting LRRK2 activation. Tyr^{1699} functions as the pivot point (fig. S11D and movie S2), and its substitution with a smaller residue would lower the energy barrier for the seesaw motion and for the transition from the inactive to the active state. The above structural observations lead us to conclude that increased conformational dynamics of G2019S, I2020T, Y1699C, N1437H, and R1441C/G/H mutations play an important role in PD pathogenesis.

The different modes of activation of LRRK2 with Rab29 or its close homologs, Rab32 or Rab38, are intriguing. Although Rab29, Rab32, and Rab38 could all activate Rab10 phosphorylation by LRRK2, only Rab29 promotes the formation of LRRK2 tetrameric assembly, boosts Ser^{1292} autophosphorylation, and is associated with late-onset PD. Moreover, LRRK2 Ser^{1292} autophosphorylation is elevated in urinary exosomes of *LRRK2* mutation carriers (46–48), but the association between Rab10 phosphorylation and *LRRK2* mutations varies across different studies (46–50). We thus speculate a pathogenic association between Rab29-dependent LRRK2 tetramerization and Ser^{1292} autophosphorylation in patients with *LRRK2* mutations. It would also be interesting to examine the Ser^{1292} autophosphorylation in PD patients with *PARK16* variations.

LRRK2 activation features a striking dimer-of-asymmetric dimer assembly containing two active core subunits encased by two inactive peripheral protomers. Intermolecular interactions between two asymmetric LRRK2 dimers stabilize the active Rab29–LRRK2 tetramer (Fig. 3, A to D). The formation of active tetramers is Rab29-dependent because such an assembly was not observed with Rab32 or without Rab29 under similar experimental conditions (Fig. 6, C and D) (10). Furthermore, Rab29 binding to the extended ARM-ANK-LRR portion of LRRK2^{cent} appears to unlock or facilitate LRRK2^{cent} activation (fig. S5A). However, the low resolution of LRRK2^{cent} ARM-ANK-LRR domains prevents us from dissecting these putative mechanisms in atomic details. Nevertheless, this Rab29- and oligomerization-controlled asymmetric activation of LRRK2 adds a new mode of kinase asymmetric activation, currently represented by EGFR (51), IRAK4 (52), and B-Raf (53, 54).

Lastly, LRRK2 activation is clearly a complex process and could be achieved by other mechanisms, such as lipid oxidation, Rab12, and microtubule-based filamentation (11, 12, 55–58). This study focuses on Rab29-induced LRRK2 activation and provides a framework for interpreting disease mutations in the context of kinase activation. Our data suggest that allosteric inhibition of LRRK2 could be potentially achieved by disrupting Rab29–LRRK2 interaction, blocking LRRK2 oligomerization, or preventing the conformational transition

from the inactive to the active states. Thus, our findings provide novel insights into LRRK2-based drug development and PD treatment.

Supplementary Material

Refer to Web version on PubMed Central for supplementary material.

Acknowledgments

We thank the support of the Cryo-Electron Microscopy Center at St. Jude Children's Research Hospital for help with cryo-EM data collection, members of the Sun lab for helpful discussion, P. Hixson for cell-culture support, M. Esmaili for initial setup of the kinase inhibition assay and P. Hixson for cross validation, N. Luo for illustrations, and I. Chen and J. Payandeh for valuable inputs for manuscript preparation. We thank the excellent technical support of the Medical Research Council (MRC) Protein Phosphorylation and Ubiquitylation Unit (PPU) DNA cloning team (coordinated by R. Toth), sequencing service (coordinated by G. Hunter), and tissue culture team (coordinated by E. Allen). We also want to thank P. Lis and the MRC PPU at the University of Dundee for their help in preparing the confocal microscopy images.

Funding:

This work was funded by the American Lebanese Syrian Associated Charities (ALSAC), NIH (R00HL143037 and R01NS129795), the UK MRC (MC_UU_00018/1) and Aligning Science Across Parkinson's (ASAP). This research was funded in part by ASAP [ASAP-000463] through the Michael J. Fox Foundation for Parkinson's Research (MJFF) to D.R.A.

This research was funded in whole or in part by the UK Medical Research Council (MC_UU_00018/1).

Data and materials availability:

The cryo-EM maps of Rab29-LRRK2 monomer, dimer, tetramers and LRRK2^{RCKW}-DNL201 complexes have been deposited in the Electron Microscopy Data Bank under accession codes EMD-29339, EMD-29341, EMD-29342, and EMD-40588. The corresponding coordinates have been deposited in the Protein Data Bank under accession codes 8FO2, 8FO8, 8FO9, and 8SMC, respectively. Raw micrographs of the Rab29-LRRK2 complex have been deposited in the Electron Microscopy Public Image Archive (EMPIAR) with accession code 47485217. Plasmids encoding constructs used for cryo-EM in this study are available upon request. All the primary immunoblotting and confocal microscopy data that are presented in this study have been deposited at Zenodo (59). Plasmids and antibodies (and associated datasheets) generated at the MRC PPU at the University of Dundee can be requested through our website: https://mrcppureagents.dundee.ac.uk/.

References and Notes

1. Lees AJ, Hardy J, Revesz T, Parkinson's disease. Lancet 373, 2055–2066 (2009). [PubMed: 19524782]
2. Tolosa E, Vila M, Klein C, Rascol O, LRRK2 in Parkinson disease: Challenges of clinical trials. Nat. Rev. Neurol 16, 97–107 (2020). [PubMed: 31980808]
3. Paisán-Ruíz C, Jain S, Evans EW, Gilks WP, Simón J, van derBrug M, López de Munain A, Aparicio S, Gil AM, Khan N, Johnson J, Martinez JR, Nicholl D, Martí Carrera I, Peña AS, de Silva R, Lees A, Martí-Massó JF, Párez-Tur J, Wood NW, Singleton AB, Cloning of the gene containing mutations that cause PARK8-linked Parkinson's disease. Neuron 44, 595–600 (2004). [PubMed: 15541308]
4. Zimprich A, Biskup S, Leitner P, Lichtner P, Farrer M, Lincoln S, Kachergus J, Hulihan M, Uitti RJ, Caine DB, Stoessl AJ, Pfeiffer RF, Patenge N, Carbajal IC, Vieregge P, Asmus F, Müller-

Myhsok B, Dickson DW, Meitinger T, Strom TM, Wszolek ZK, Gasser T, Mutations in LRRK2 cause autosomal-dominant parkinsonism with pleomorphic pathology. Neuron 44, 601–607 (2004). [PubMed: 15541309]

5. Ramírez MB, Madero-Perez J, Rivero-Rios P, Martinez-Salvador M, Lara Ordonez AJ, Fernandez B, Fdez E, Hilfiker S, LRRK2 and Parkinson's disease: From lack of structure to gain of function. Curr. Protein Pept. Sci 18, 677–686 (2017). [PubMed: 26965688]
6. Bryant N, Malpeli N, Ziaee J, Blauwendraat C, Liu Z, West AB; AMP PD Consortium, Identification of LRRK2 missense variants in the accelerating medicines partnership Parkinson's disease cohort. Hum. Mol. Genet 30, 454–466 (2021). [PubMed: 33640967]
7. Kalogeropulou AF, Purlyte E, Tonelli F, Lange SM, Wightman M, Prescott AR, Padmanabhan S, Sammler E, Alessi DR, Impact of 100 LRRK2 variants linked to Parkinson's disease on kinase activity and microtubule binding. Biochem. J 479, 1759–1783 (2022). [PubMed: 35950872]
8. Usmani A, Shavarebi F, Hiniker A, The cell biology of LRRK2 in Parkinson's disease. Mol. Cell. Biol 41, e00660–20 (2021). [PubMed: 33526455]
9. Deniston CK, Salogiannis J, Mathea S, Snead DM, Lahiri I, Matyszewski M, Donosa O, Watanabe R, Bohning J, Shiau AK, Knapp S, Villa E, Reck-Peterson SL, Leschziner AE, Structure of LRRK2 in Parkinson's disease and model for microtubule interaction. Nature 588, 344–349 (2020). [PubMed: 32814344]
10. Myasnikov A, Zhu H, Hixson P, Xie B, Yu K, Pitre A, Peng J, Sun J, Structural analysis of the full-length human LRRK2. Cell 184, 3519–3527.e10 (2021). [PubMed: 34107286]
11. Watanabe R, Buschauer R, Böhning J, Audagnotto M, Lasker K, Lu T-W, Boassa D, Taylor S, Villa E, The in situ structure of Parkinson's disease-linked LRRK2. Cell 182, 1508–1518.e16 (2020). [PubMed: 32783917]
12. Snead DM, Matyszewski M, Dickey AM, Lin YX, Leschziner AE, Reck-Peterson SL, Structural basis for Parkinson's disease-linked LRRK2's binding to microtubules. Nat. Struct. Mol. Biol 29, 1196–1207 (2022). [PubMed: 36510024]
13. Weng JH, Trilling CR, Kaila Sharma P, Störmer E, Wu J, Herberg FW, Taylor SS, Novel LRR-ROC motif that links the N- and C-terminal domains in LRRK2 undergoes an order-disorder transition upon activation. J. Mol. Biol 435, 167999 (2023). [PubMed: 36764356]
14. Weng JH, Ma W, Wu J, Sharma PK, Silletti S, McCammon JA, Taylor S, Capturing differences in the regulation of LRRK2 dynamics and conformational states by small molecule kinase inhibitors. ACS Chem. Biol 18, 810–821 (2023). [PubMed: 37043829]
15. Weng JH, Aoto PC, Lorenz R, Wu J, Schmidt SH, Manschwetus JT, Kaila-Sharma P, Silletti S, Mathea S, Chatterjee D, Knapp S, Herberg FW, Taylor SS, LRRK2 dynamics analysis identifies allosteric control of the crosstalk between its catalytic domains. PLOS Biol. 20, e3001427 (2022). [PubMed: 35192607]
16. Schmidt SH, Weng J-H, Aoto PC, Boassa D, Mathea S, Silletti S, Hu J, Wallbott M, Komives EA, Knapp S, Herberg FW, Taylor SS, Conformation and dynamics of the kinase domain drive subcellular location and activation of LRRK2. Proc. Natl. Acad. Sci. U.S.A 118, e2100844118 (2021). [PubMed: 34088839]
17. Pfeffer SR, LRRK2 phosphorylation of Rab GTPases in Parkinson's disease. FEBS Lett. 597, 811–818 (2023). [PubMed: 36114007]
18. Pfeffer SR, LRRK2 and Rab GTPases. Biochem. Soc. Trans 46, 1707–1712 (2018). [PubMed: 30467121]
19. Kuwahara T, Iwatsubo T, The emerging functions of LRRK2 and Rab GTPases in the endolysosomal system. Front. Neurosci 14, 227 (2020). [PubMed: 32256311]
20. Ebanks K, Lewis PA, Bandopadhyay R, Vesicular dysfunction, and the pathogenesis of Parkinson's disease: Clues From Genetic Studies. Front. Neurosci 13, 1381 (2020). [PubMed: 31969802]
21. Kalogeropulou AF, Freemantle JB, Lis P, Vides EG, Polinski NK, Alessi DR, Endogenous Rab29 does not impact basal or stimulated LRRK2 pathway activity. Biochem. J 477, 4397–4423 (2020). [PubMed: 33135724]
22. Kuwahara T, Inoue K, D'Agati VD, Fujimoto T, Eguchi T, Saha S, Wolozin B, Iwatsubo T, Abeliovich A, LRRK2 and RAB7L1 coordinately regulate axonal morphology and lysosome integrity in diverse cellular contexts. Sci. Rep 6, 29945 (2016). [PubMed: 27424887]

23. Fujimoto T, Kuwahara T, Eguchi T, Sakurai M, Komori T, Iwatsubo T, Parkinson's disease-associated mutant LRRK2 phosphorylates Rab7L1 and modifies trans-Golgi morphology. Biochem. Biophys. Res. Commun 495, 1708–1715 (2018). [PubMed: 29223392]
24. Liu Z, Bryant N, Kumaran R, Beilina A, Abeliovich A, Cookson MR, West AB, LRRK2 phosphorylates membrane-bound Rabs and is activated by GTP-bound Rab7L1 to promote recruitment to the trans-Golgi network. Hum. Mol. Genet 27, 385–395 (2018). [PubMed: 29177506]
25. McGrath E, Waschbiisch D, Baker BM, Khan AR, LRRK2 binds to the Rab32 subfamily in a GTP-dependent manner via its armadillo domain. Small GTPases 12, 133–146 (2021). [PubMed: 31552791]
26. Beilina A, Rudenko IN, Kaganovich A, Civiero L, Chau H, Kalia SK, Kalia LV, Lobbestael E, Chia R, Ndukwe K, Ding J, Nalls MA, Olszewski M, Hauser DN, Kumaran R, Lozano AM, Baekelandt V, Greene LE, Taymans J-M, Greggio E, Cookson MR, Nalls MA, Plagnol V, Martinez M, Hernandez DG, Sharma M, Sheerin U-M, Saad M, Simón-Sánchez J, Schulte C, Lesage S, Sveinbjörnsdóttir S, Arepalli S, Barker R, Ben-Shlomo Y, Berendse HW, Berg D, Bhatia K, de Bie RMA, Biffi A, Bloem B, Bochdanovits Z, Bonin M, Bras JM, Brockmann K, Brooks J, Burn DJ, Charlesworth G, Chen H, Chong S, Clarke CE, Cookson MR, Cooper JM, Corvol JC, Counsell C, Damier P, Dartigues J-F, Deloukas P, Deuschl G, Dexter DT, van Dijk KD, Dillman A, Durif F, Dürr A, Edkins S, Evans JR, Foltynie T, Gao J, Gardner M, Gibbs JR, Goate A, Gray E, Guerreiro R, Gústafsson Ó, Harris C, van Hilten JJ, Hofman A, Hollenbeck A, Holton J, Hu M, Huang X, Huber H, Hudson G, Hunt SE, Huttenlocher J, Illig T, München HZ, Jónsson PV, Lambert J-C, Langford C, Lees A, Lichtner P, München HZ, Limousin P, Lopez G, Lorenz D, McNeill A, Moorby C, Moore M, Morris HR, Morrison KE, Mudanohwo E, O'Sullivan SS, Pearson J, Perlmutter JS, Pétursson H, Pollak P, Post B, Potter S, Ravina B, Revesz T, Riess O, Rivadeneira F, Rizzu P, Ryten M, Sawcer S, Schapira A, Scheffer H, Shaw K, Shoulson I, Sidransky E, Smith C, Spencer CCA, Stefánsson H, Steinberg S, Stockton JD, Strange A, Talbot K, Tanner CM, Tashakkori-Ghanbaria A, Tison F, Trabzuni D, Traynor BJ, Uitterlinden AG, Velseboer D, Vidailhet M, Walker R, van de Warrenburg B, Wickremaratchi M, Williams N, Williams-Gray CH, Winder-Rhodes S, Stefánsson K, Hardy J, Heutink P, Brice A, Gasser T, Singleton AB, Wood NW, Chinnery PF, Arepalli S, Cookson MR, Dillman A, Ferrucci L, Gibbs JR, Hernandez DG, Johnson R, Longo DL, Majounie E, Nalls MA, O'Brien R, Singleton AB, Traynor BJ, Troncoso J, van der Brug M, Zielke HR, Zonderman AB, International Parkinson's Disease Genomics Consortium, North American Brain Expression Consortium, Unbiased screen for interactors of leucine-rich repeat kinase 2 supports a common pathway for sporadic and familial Parkinson disease. Proc. Natl. Acad. Sci. U.S.A 111, 2626–2631 (2014). [PubMed: 24510904]
27. MacLeod DA, Rhinn H, Kuwahara T, Zolin A, Di Paolo G, McCabe BD, Marder KS, Honig LS, Clark LN, Small SA, Abeliovich A, RAB7L1 interacts with LRRK2 to modify intraneuronal protein sorting and Parkinson's disease risk. Neuron 77, 425–439 (2013). [PubMed: 23395371]
28. Purlyte E, Dhekne HS, Sarhan AR, Gomez R, Lis P, Wightman M, Martinez TN, Tonelli F, Pfeffer SR, Alessi DR, Rab29 activation of the Parkinson's disease-associated LRRK2 kinase. EMBO J. 37, 1–18 (2018). [PubMed: 29212815]
29. Berwick DC, Heaton GR, Azeggagh S, Harvey K, LRRK2 Biology from structure to dysfunction: Research progresses, but the themes remain the same. Mol. Neurodegener 14, 49 (2019). [PubMed: 31864390]
30. Gomez RC, Wawro P, Lis P, Alessi DR, Pfeffer SR, Membrane association but not identity is required for LRRK2 activation and phosphorylation of Rab GTPases. J. Cell Biol 218, 4157–4170 (2019). [PubMed: 31624137]
31. Waschbüsch D, Michels H, Strassheim S, Ossendorf E, Kessler D, Gloeckner CJ, Barnekow A, LRRK2 transport is regulated by its novel interacting partner Rab32. PLOS ONE 9, e111632 (2014). [PubMed: 25360523]
32. Pylypenko O, Hammich H, Yu IM, Houdusse A, Rab GTPases, and their interacting protein partners: Structural insights into Rab functional diversity. Small GTPases 9, 22–48 (2018). [PubMed: 28632484]
33. Vides EG, Adhikari A, Chiang CY, Lis P, Purlyte E, Limouse C, Shumate JL, Spínola-Lasso E, Dhekne HS, Alessi DR, Pfeffer SR, A feed-forward pathway drives LRRK2 kinase membrane recruitment and activation. eLife 11, e79771 (2022). [PubMed: 36149401]

34. Steger M, Diez F, Dhekne HS, Lis P, Nirujogi RS, Karayel O, Tonelli F, Martinez TN, Lorentzen E, Pfeffer SR, Alessi DR, Mann M, Systematic proteomic analysis of LRRK2-mediated Rab GTPase phosphorylation establishes a connection to ciliogenesis. eLife 6, e31012 (2017). [PubMed: 29125462]
35. Taylor SS, Kaila-Sharma P, Weng J-H, Aoto P, Schmidt SH, Knapp S, Mathea S, Herberg FW, Kinase domain is a dynamic hub for driving LRRK2 allostery. Front. Mol. Neurosci 13, 538219 (2020). [PubMed: 33122997]
36. Biosa A, Trancikova A, Civiero L, Glauser L, Bubacco L, Greggio E, Moore DJ, GTPase activity regulates kinase activity and cellular phenotypes of Parkinson's disease-associated LRRK2. Hum. Mol. Genet 22, 1140–1156 (2013). [PubMed: 23241358]
37. Taymans JM, Vancraenenbroeck R, Ollikainen P, Beilina A, Lobbestael E, De Maeyer M, Baekelandt V, Cookson MR, LRRK2 kinase activity is dependent on LRRK2 GTP binding capacity but independent of LRRK2 GTP binding. PLOS ONE 6, e23207 (2011). [PubMed: 21858031]
38. West AB, Moore DJ, Choi C, Andrabi SA, Li X, Dikeman D, Biskup S, Zhang Z, Lim K-L, Dawson VL, Dawson TM, Parkinson's disease-associated mutations in LRRK2 link enhanced GTP-binding and kinase activities to neuronal toxicity. Hum. Mol. Genet 16, 223–232 (2007). [PubMed: 17200152]
39. Ito G, Okai T, Fujino G, Takeda K, Ichijo H, Katada T, Iwatsubo T, GTP binding is essential to the protein kinase activity of LRRK2, a causative gene product for familial Parkinson's disease. Biochemistry 46, 1380–1388 (2007). [PubMed: 17260967]
40. Jennings D, Huntwork-Rodriguez S, Henry AG, Sasaki JC, Meisner R, Diaz D, Solanoy H, Wang X, Negrou E, Bondar VV, Ghosh R, Maloney MT, Propson NE, Zhu Y, Maciuca RD, Harris L, Kay A, LeWitt P, King TA, Kern D, Ellenbogen A, Goodman I, Siderowf A, Aldred J, Omidvar O, Masoud ST, Davis SS, Arguello A, Estrada AA, de Vicente J, Sweeney ZK, Astarita G, Borin MT, Wong BK, Wong H, Nguyen H, Scearce-Levie K, Ho C, Troyer MD, Preclinical and clinical evaluation of the LRRK2 inhibitor DNL201 for Parkinson's disease. Sci. Transl. Med 14, eabj2658 (2022). [PubMed: 35675433]
41. Tasegian A, Singh F, Ganley IG, Reith AD, Alessi DR, Impact of Type II LRRK2 inhibitors on signaling and mitophagy. Biochem. J 478, 3555–3573 (2021). [PubMed: 34515301]
42. Rivero-Ríos P, Romo-Lozano M, Fernández B, Fdez E, Hilfiker S, Distinct roles for Rab10 and Rab29 in pathogenic LRRK2-mediated endolysosomal trafficking alterations. Cells 9, 1719 (2020). [PubMed: 32709066]
43. Fellgett A, Middleton CA, Munns J, Ugbode C, Jaciuch D, Wilson LG, Chawla S, Elliott CJH, Multiple pathways of LRRK2-G2019S/Rab10 interaction in dopaminergic neurons. J. Parkinsons Dis 11, 1805–1820 (2021). [PubMed: 34250948]
44. Cinapanta A, Shavarebi F, Porath J, Shen Y, Balen C, Nguyen A, Tseng J, Leong WS, Liu M, Lis P, Di Pietro SM, Hiniker A, Endogenous Rab38 regulates LRRK2's membrane recruitment and substrate Rab phosphorylation in melanocytes. J. Biol. Chem 299, 105192 (2023). [PubMed: 37625589]
45. Christensen KV, Hentzer M, Oppermann FS, Elschenbroich S, Dossang P, Thirstup K, Egebjerg J, Williamson DS, Smith GP, LRRK2 exonic variants associated with Parkinson's disease augment phosphorylation levels for LRRK2-Ser1292 and Rab10-Thr73. bioRxiv 447946 [Preprint] (2018). 10.1101/447946.
46. Fan Y, Nirujogi RS, Garrido A, Ruiz-Martínez J, Bergareche-Yarza A, Mondragón-Rezola E, Vinagre-Aragón A, Croitoru I, Gorostidi Pagola A, Paternain Markinez L, Alcalay R, Hickman RA, Düring J, Gomes S, Pratuseviciute N, Padmanabhan S, Valldeoriola F, Pérez Sisqués L, Malagelada C, Ximelis T, Molina Porcel L, Martí MJ, Tolosa E, Alessi DR, Sammler EM, R1441G but not G2019S mutation enhances LRRK2 mediated Rab10 phosphorylation in human peripheral blood neutrophils. Acta Neuropathol. 142, 475–494 (2021). [PubMed: 34125248]
47. Fan Y, Howden AJM, Sarhan AR, Lis P, Ito G, Martinez TN, Brockmann K, Gasser T, Alessi DR, Sammler EM, Interrogating Parkinson's disease LRRK2 kinase pathway activity by assessing Rab10 phosphorylation in human neutrophils. Biochem. J 475, 23–44 (2018). [PubMed: 29127255]

48. Garrido A, Santamaría E, Fernández-Irigoyen J, Soto M, Simonet C, Fernández M, Obiang D, Tolosa E, Martí M-J, Padmanabhan S, Malagelada C, Ezquerra M, Fernández-Santiago R, Differential phospho-signatures in blood cells identify LRRK2 G2019S carriers in Parkinson's disease. Mov. Disord 37, 1004–1015 (2022). [PubMed: 35049090]
49. Atashrazm F, Hammond D, Perera G, Bolliger MF, Matar E, Halliday GM, Schüle B, Lewis SJG, Nichols RJ, Dzamko N, LRRK2-mediated Rab10 phosphorylation in immune cells from Parkinson's disease patients. Mov. Disord 34, 406–415 (2019). [PubMed: 30597610]
50. Karayel Ö, Tonelli F, Virreira Winter S, Geyer PE, Fan Y, Sammler EM, Alessi DR, Steger M, Mann M, Accurate MS-based Rab10 phosphorylation stoichiometry determination as readout for LRRK2 activity in Parkinson's disease. Mol. Cell. Proteomics 19, 1546–1560 (2020). [PubMed: 32601174]
51. Zhang X, Gureasko J, Shen K, Cole PA, Kuriyan J, An allosteric mechanism for activation of the kinase domain of epidermal growth factor receptor. Cell 125, 1137–1149 (2006). [PubMed: 16777603]
52. Ferrao R, Zhou H, Shan Y, Liu Q, Li Q, Shaw DE, Li X, Wu H, IRAK4 dimerization and trans-autophosphorylation are induced by Myddosome assembly. Mol. Cell 55, 891–903 (2014). [PubMed: 25201411]
53. Kondo Y, Ognjenović J, Baneijee S, Karandur D, Merk A, Kulhanek K, Wong K, Roose JP, Subramaniam S, Kuriyan J, Cryo-EM structure of a dimeric B-Raf:14-3-3 complex reveals asymmetry in the active sites of B-Raf kinases. Science 366, 109–115 (2019). [PubMed: 31604311]
54. Park E, Rawson S, Li K, Kim B-W, Ficarro SB, Pino GG-D, Sharif H, Marto JA, Jeon H, Eck MJ, Architecture of autoinhibited and active BRAF-MEK1-14-3-3 complexes. Nature 575, 545–550 (2019). [PubMed: 31581174]
55. Schmidt SH, Knape MJ, Boassa D, Mumdey N, Kornev AP, Ellisman MH, Taylor SS, Herberg FW, The dynamic switch mechanism that leads to activation of LRRK2 is embedded in the DFGψ motif in the kinase domain. Proc. Natl. Acad. Sci. U.S.A 116, 14979–14988 (2019). [PubMed: 31292254]
56. Bondar VV, Wang X, Davis OB, Maloney MT, Agam M, Chin MY, Cheuk-NgaHo A, Joy D, Lewcock JW, Di Paolo G, Thorne RG, Sweeney ZK, Henry AG, Rab12 regulates LRRK2 activity by promoting its localization to lysosomes. bioRxiv 2023.02.21.529466 [Preprint] (2023). 10.1101/2023.02.21.529466.
57. Dhekne HS, Tonelli F, Yeshaw WM, Chiang CY, Limouse C, Jaimon E, Purlyte E, Alessi DR, Pfeffer SR, Genome-wide screen reveals Rab12 GTPase as a critical activator of pathogenic LRRK2 kinase. bioRxiv 2023.02.17.529028 [Preprint] (2023). 10.1101/2023.02.17.529Q28
58. Di Maio R, Hoffman EK, Rocha EM, Keeney MT, Sanders LH, De Miranda BR, Zharikov A, Van Laar A, Stepan AF, Lanz TA, Kofler JK, Burton EA, Alessi DR, Hastings TG, Greenamyre JT, LRRK2 activation in idiopathic Parkinson's disease. Sci. Transl. Med 10, eaar5429 (2018). [PubMed: 30045977]
59. Tonelli F, Structural basis of LRRK2 membrane recruitment and activation, Version v2, Zenodo (2023); 10.5281/zenodo.7601062.
60. Goehring A, Lee C-H, Wang KH, Michel JC, Claxton DP, Baconguis I, Althoff T, Fischer S, Garcia KC, Gouaux E, Screening and large-scale expression of membrane proteins in mammalian cells for structural studies. Nat. Protoc 9, 2574–2585 (2014). [PubMed: 25299155]
61. Kirchhofer A, Helma J, Schmidthals K, Frauer C, Cui S, Karcher A, Pellis M, Muyldermans S, Casas-Delucchi CS, Cardoso MC, Leonhardt H, Hopfner K-P, Rothbauer U, Modulation of protein properties in living cells using nanobodies. Nat. Struct. Mol. Biol 17, 133–138 (2010). [PubMed: 20010839]
62. Zheng SQ, Palovcak E, Armache J-P, Verba KA, Cheng Y, Agard DA, MotionCor2: Anisotropic correction of beam-induced motion for improved cryo-electron microscopy. Nat. Methods 14, 331–332 (2017). [PubMed: 28250466]
63. Zhang K, Gctf: Real-time CTF determination and correction. J. Struct. Biol 193, 1–12 (2016). [PubMed: 26592709]

64. Punjani A, Rubinstein JL, Fleet DJ, Brubaker MA, cryoSPARC: Algorithms for rapid unsupervised cryo-EM structure determination. Nat. Methods 14, 290–296 (2017). [PubMed: 28165473]

65. Henderson R, Sali A, Baker ML, Carragher B, Devkota B, Downing KH, Egelman EH, Feng Z, Frank J, Grigorieff N, Jiang W, Ludtke SJ, Medalia O, Penczek PA, Rosenthal PB, Rossmann MG, Schmid MF, Schröder GF, Steven AC, Stokes DL, Westbrook JD, Wriggers W, Yang H, Young J, Berman HM, Chiu W, Kleywegt GJ, Lawson CL, Outcome of the first electron microscopy validation task force meeting. Structure 20, 205–214 (2012). [PubMed: 22325770]

66. Bepler T, Morin A, Rapp M, Brasch J, Shapiro L, Noble AJ, Berger B, Positive-unlabeled convolutional neural networks for particle picking in cryo-electron micrographs. Nat. Methods 16, 1153–1160 (2019). [PubMed: 31591578]

67. Jumper J, Evans R, Pritzel A, Green T, Figumov M, Ronneberger O, Tunyasuvunakool K, Bates R, Žídek A, Potapenko A, Bridgland A, Meyer C, Kohl SAA, Ballard AJ, Cowie A, Romera-Paredes B, Nikolov S, Jain R, Adler J, Back T, Petersen S, Reiman D, Clancy E, Zielinski M, Steinegger M, Pacholska M, Berghammer T, Bodenstein S, Silver D, Vinyals O, Senior AW, Kavukcuoglu K, Kohli P, Hassabis D, Highly accurate protein structure prediction with AlphaFold. Nature 596, 583–589 (2021). [PubMed: 34265844]

68. Pettersen EF, Goddard TD, Huang CC, Couch GS, Greenblatt DM, Meng EC, Ferrin TE, UCSF Chimera—A visualization system for exploratory research and analysis. J. Comput. Chem 25, 1605–1612 (2004). [PubMed: 15264254]

69. Emsley P, Lohkamp B, Scott WG, Cowtan K, Features and development of Coot. Acta Crystallogr. D 66, 486–501 (2010). [PubMed: 20383002]

70. Adams PD, Afonine PV, Bunkóczi G, Chen VB, Davis IW, Echols N, Headd JJ, Hung L-W, Kapral GJ, Grosse-Kunstleve RW, McCoy AJ, Moriarty NW, Oeffner R, Read RJ, Richardson DC, Richardson JS, Terwilliger TC, Zwart PH, PHENIX: A comprehensive Python-based system for macromolecular structure solution. Acta Crystallogr. D 66, 213–221 (2010). [PubMed: 20124702]

71. Chen VB, Arendall WB 3rd, Headd JJ, Keedy DA, Immormino RM, Kapral GJ, Murray LW, Richardson JS, Richardson DC, MolProbity: All-atom structure validation for macromolecular crystallography. Acta Crystallogr. D 66, 12–21 (2010). [PubMed: 20057044]

72. Goddard TD, Huang CC, Meng EC, Pettersen EF, Couch GS, Morris JH, Ferrin TE, UCSF ChimeraX: Meeting modern challenges in visualization and analysis. Protein Sci. 27, 14–25 (2018). [PubMed: 28710774]

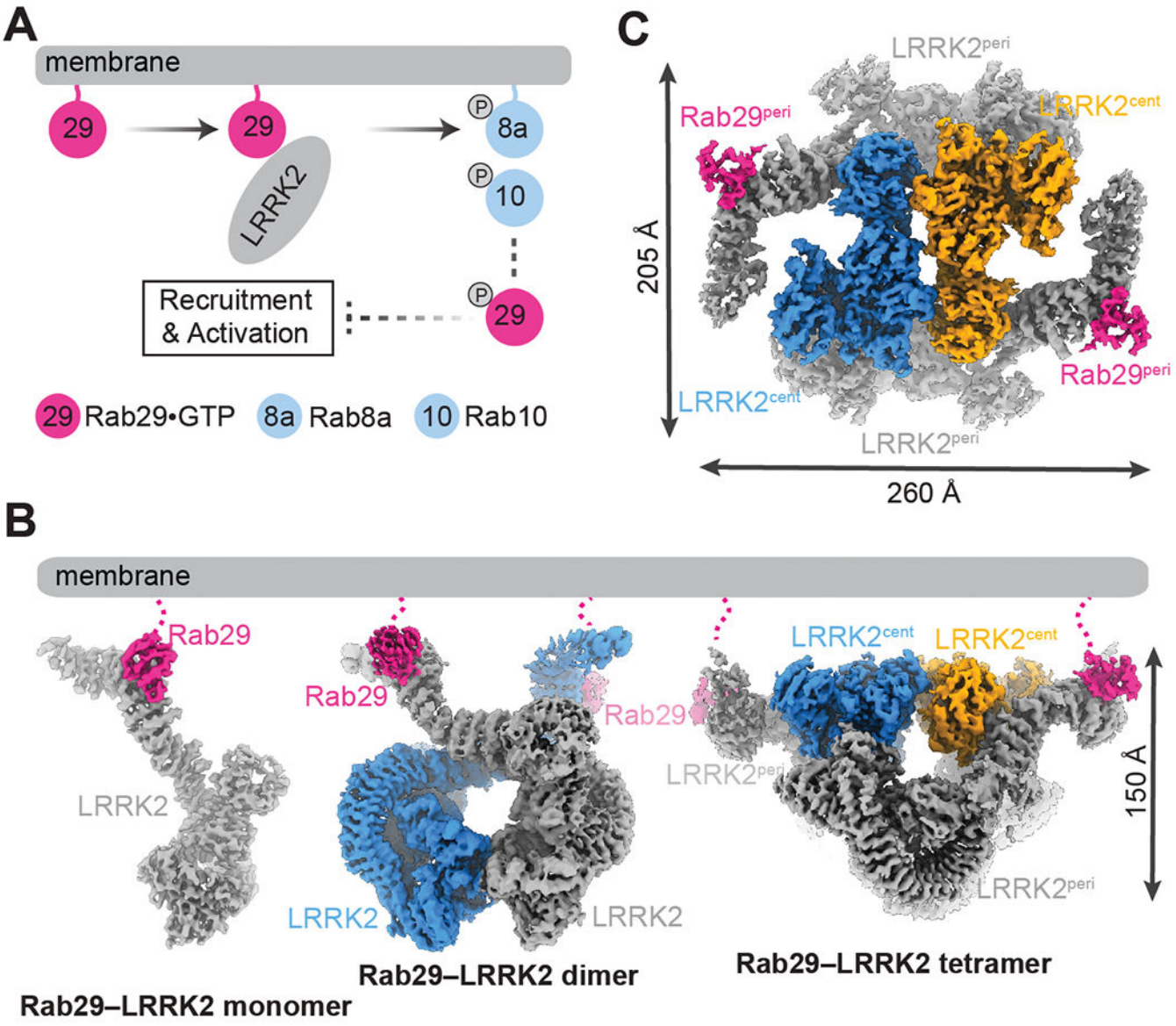

Fig. 1. Structural determination of the Rab29–LRRK2 complex.

(**A**) Schematic diagram showing Rab29-mediated LRRK2 membrane recruitment and activation. (**B**) Cryo-EM structures of the Rab29–LRRK2 complex in three oligomerization states. (**C**) Top view of the cryo-EM structure of the Rab29–LRRK2 tetramer.

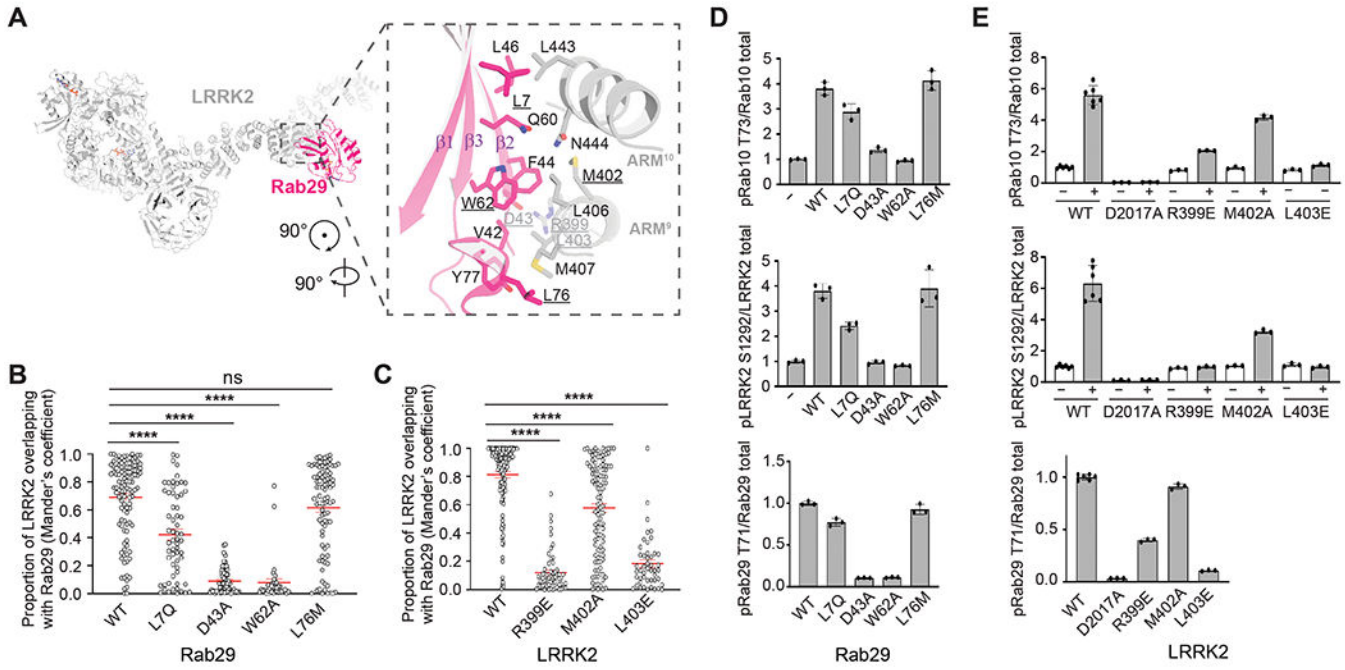

Fig. 2. Molecular basis of Rab29-dependent LRRK2 recruitment.

(**A**) Rab29–LRRK2 interface in the LRRK2 monomer state. LRRK2 and Rab29 are colored gray and hot pink, respectively. Side chains of interface residues are shown as sticks. (**B** and **C**) Impact of Rab29 or LRRK2 mutations on LRRK2 localization in HEK293 cells. Quantification of a portion of LRRK2 overlapping with Rab29 according to Mander's coefficient for confocal analysis is shown in fig. S3, A and B. Each empty circle represents colocalization coefficient (Mander's coefficient) measured in one cell. Error bars represent SEM. Significance was determined by the Kruskal-Wallis one-way analysis of variance (ANOVA) test. **** $P < 0.0001$; ns (not significant). (**D** and **E**) Quantification of the immunoblotting data shown in fig. S3, C and D. Data are presented as ratios of pRab10-Thr^{73}/total Rab10, pLRRK2-Ser^{1292}/total LRRK2, and pRab29-Thr^{71}/total Rab29, normalized to the average of LRRK2 WT values. The data shown are the mean ± SD of three determinations. Single-letter abbreviations for the amino acid residues are as follows: A, Ala; C, Cys; D, Asp; E, Glu; F, Phe; G, Gly; H, His; I, Ile; K, Lys; L, Leu; M, Met; N, Asn; P, Pro; Q, Gln; R, Arg; S, Ser; T, Thr; V, Val; W, Trp; and Y, Tyr.

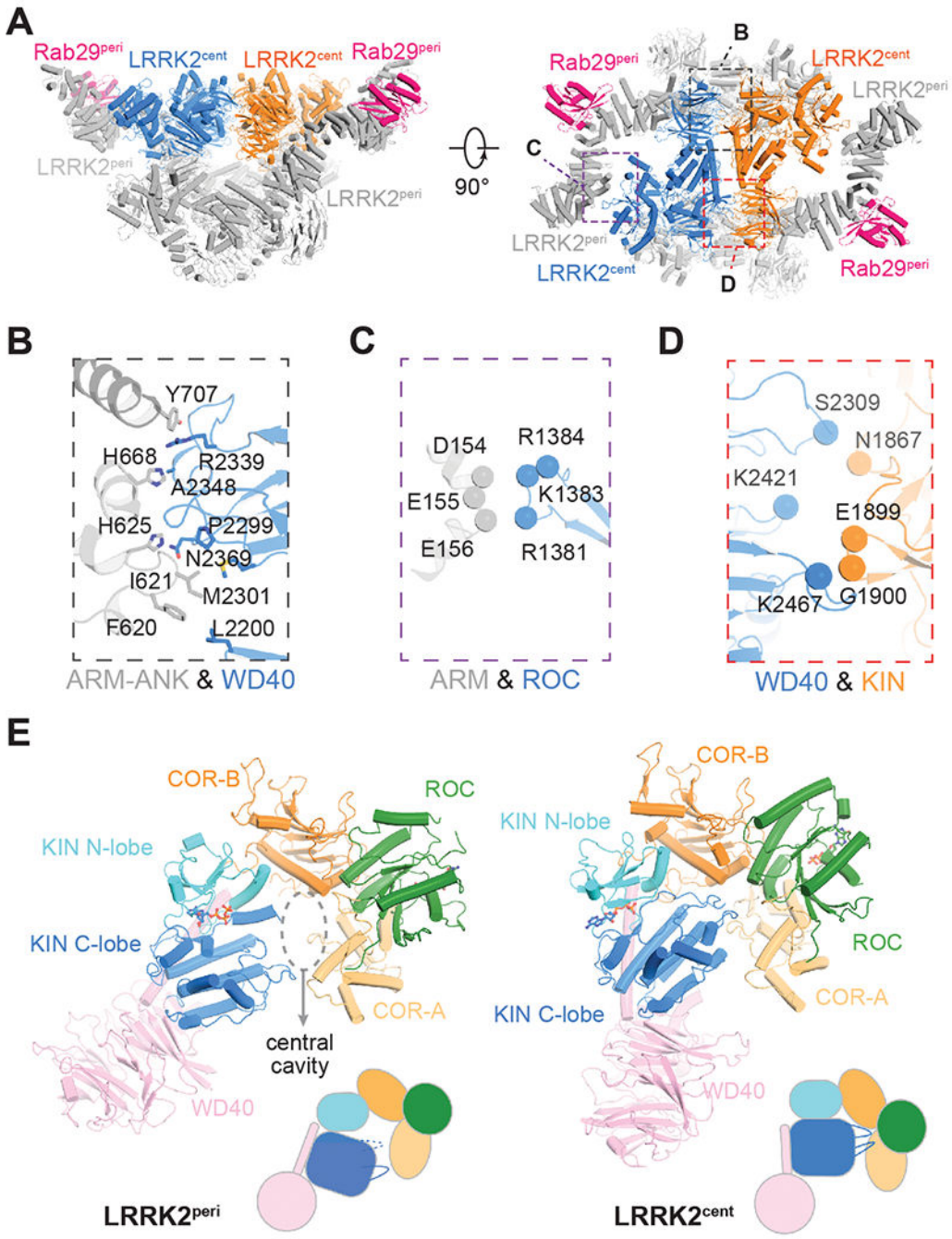

Fig. 3. Structure of the Rab29–LRRK2 tetramer.

(**A**) Cryo-EM structure of the Rab29–LRRK2 tetramer with two different views. Peripheral Rab29 (Rab29^{peri}) and LRRK2 (LRRK2^{peri}) are colored in hot pink and gray, respectively; central LRRK2 (LRRK2^{cent}) copies are colored in blue and orange. (**B** and **C**) Interactions between (B) the WD40 domain of LRRK2^{cent} and ARM-ANK domains of LRRK2^{peri} and (C) the ROC domain of LRRK2^{cen} and the ARM domain of LRRK2^{peri}. (**D**) Interactions between two LRRK2^{cent} copies. (**E**) Conformational changes in the C-terminal halves of LRRK2 upon activation. A dashed circle indicates the central cavity between the KIN and

COR domains. Color codes for different parts of LRRK2 are as follows: ROC, green; COR-A, light orange; COR-B, bright orange; N-lobe of KIN, cyan; C-lobe of KIN, marine; WD40, pink.

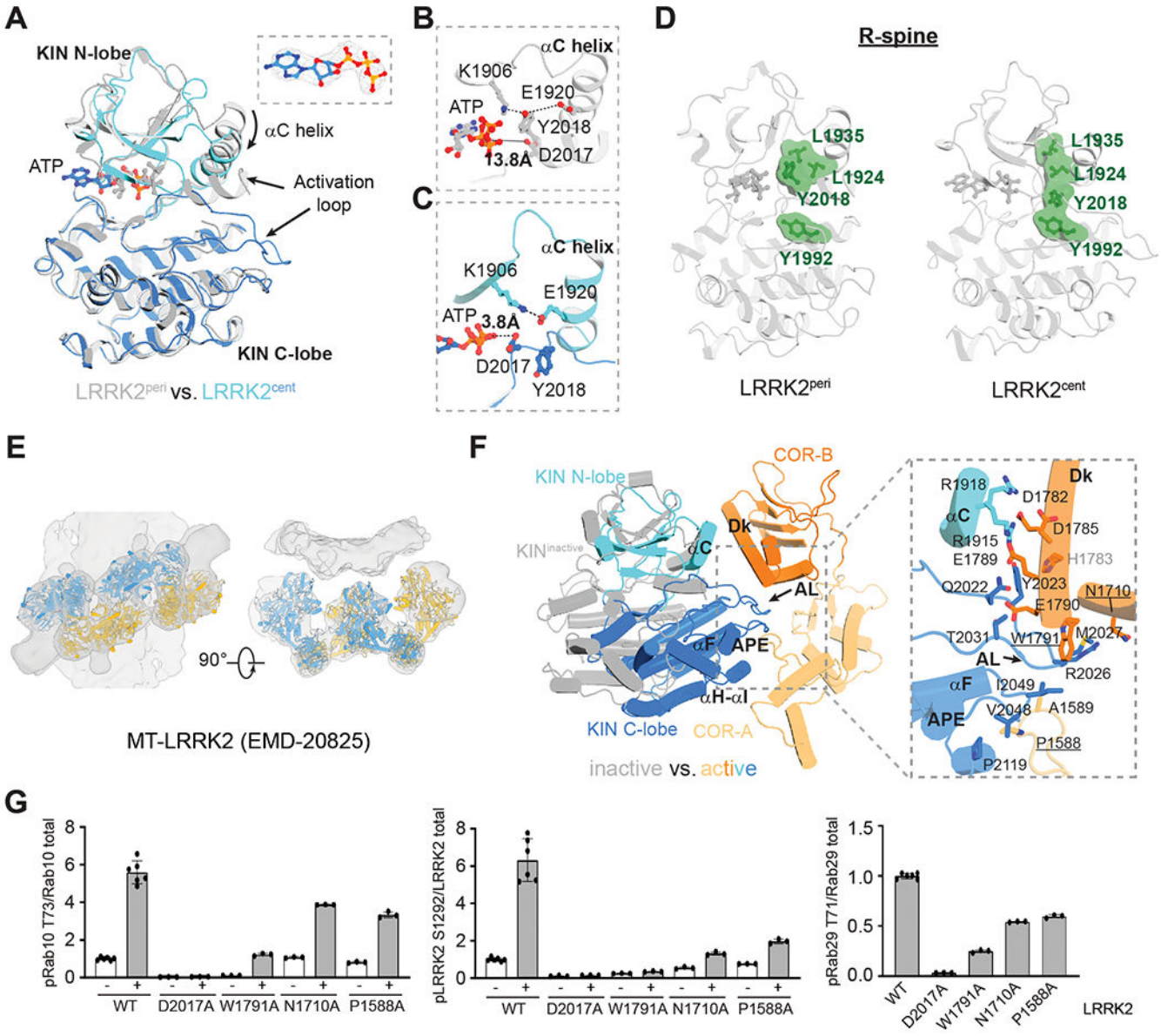

Fig. 4. An active conformation of LRRK2.

(**A**) Superposition of kinase domains of LRRK2^{cent} and LRRK2^{peri}. N- and C-lobes of the LRRK2^{cent} kinase domain are colored in cyan and marine, respectively; the LRRK2^{peri} KIN domain is colored in gray. (Inset) Image shows the Cryo-EM density of the ATP molecule. (**B** and **C**) Key catalytic residues in LRRK2^{peri} (B) and LRRK2^{cent} (C) KIN domain with side chains shown as ball-and-stick models. The distances between the side chain of D2017 and the phosphate group of ATP are indicated with dashed lines. (**D**) R-spine of the LRRK2^{peri} (left) and LRRK2^{cent} (right) KIN domains. The four residues forming the R-spine (L1935, L1924, Y2018, and Y1992) are shown as green surfaces. (**E**) Docking of C-terminal catalytic halves of LRRK2^{cent} into the cryo-ET map of microtubule-bound LRRK2. (**F**) Movement of the KIN domain relative to the COR domain upon activation. (Inset) Interactions between the KIN and COR domains in the active conformation; side

chains of the interface residues are shown as sticks. Dk, docking helix; APE, conserved APE motif; AL, activation loop. (**G**) Quantitative immunoblotting analysis of the cellular kinase activity of LRRK2-bearing mutations in the interface between the KIN and COR domains in fig. S6C. Data are presented as ratios of pRab10-Thr^{73}/total Rab10, pLRRK2-Ser^{1292}/total LRRK2, and pRab29-Thr^{71}/total Rab29, normalized to the average of LRRK2 WT values. The data shown are the mean ± SD of three experiments.

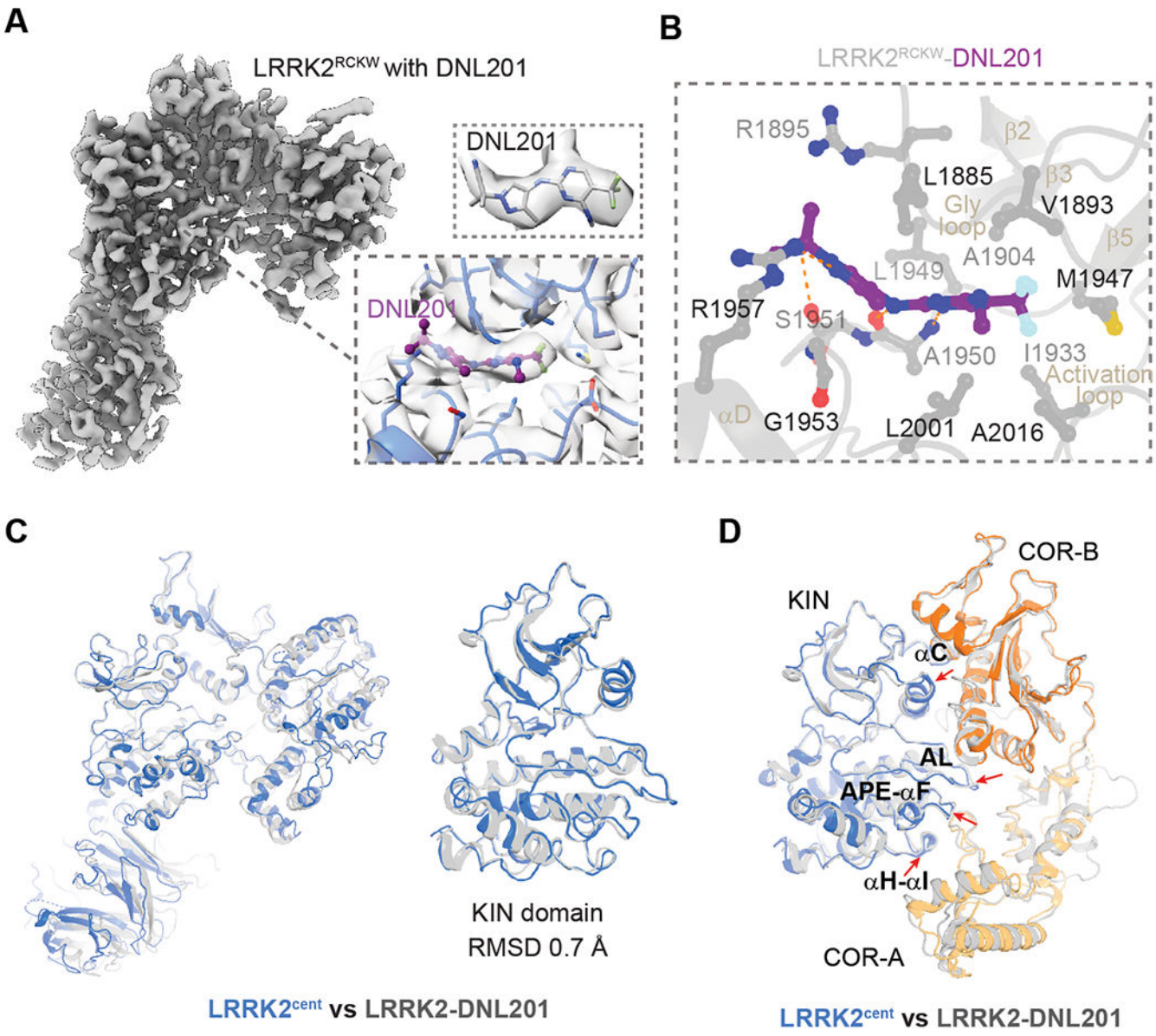

Fig. 5. Structure of LRRK2^{RCKW} with DNL201.

(**A**) Cryo-EM map of LRRK2^{RCKW} in complex with type I inhibitor DNL201. (Insets) Cryo-EM densities of the DNL201 inhibitor (top) and the surrounding residues (bottom) are shown. (**B**) DNL201 binding site [magnified from bottom inset of (A)]. Side chains of DNL201-interacting residues are shown as sticks. (**C**) Structural comparison of DNL201-bound LRRK2^{RCKW} and LRRK2^{cent} structures. (**D**) Comparison of KIN-ROC interface between LRRK2^{RCKW}-DNL201 (gray) and LRRK2^{cent} (blue and orange). Key structural elements from KIN domain involved in the interaction are labeled.

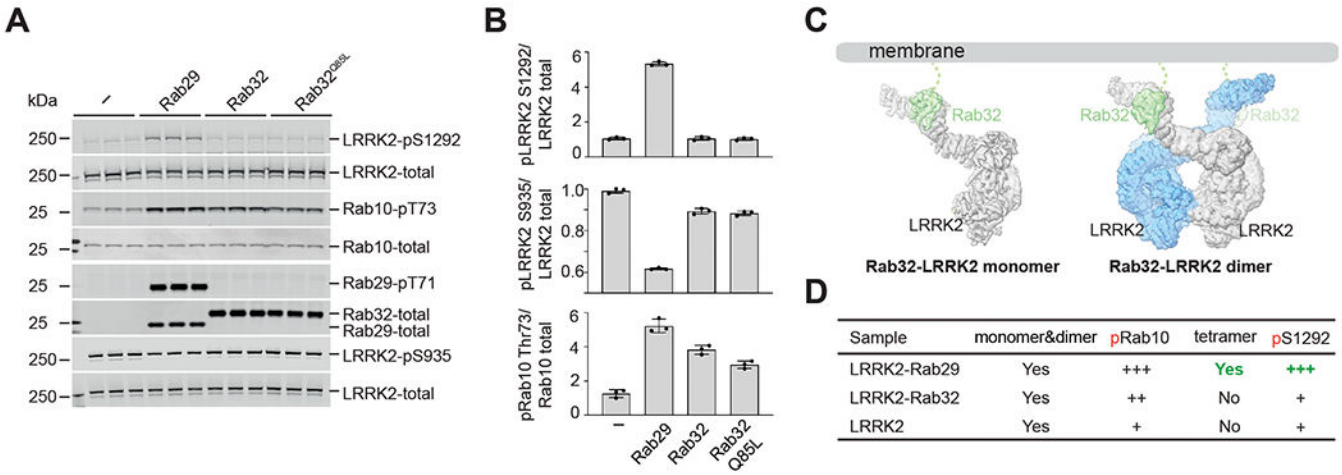

Sample	monomer&dimer	pRab10	tetramer	pS1292
LRRK2-Rab29	Yes	+++	Yes	+++
LRRK2-Rab32	Yes	++	No	+
LRRK2	Yes	+	No	+

Fig. 6. Rab29-LRRK2 tetramer and kinase activation.

(**A** and **B**) Quantitative immunoblotting analysis of the cellular kinase activity of LRRK2 in the presence of Rab29 or Rab32. HEK293 cells were transiently cotransfected with WT LRRK2 and hemagglutinin (HA)–tagged empty vector ("–"), HA-tagged Rab29, or HA-tagged Rab32 (WT or Q85L mutant). Data are presented as ratios of pLRRK2-Ser^{1292}/total LRRK2, pRab10-Thr^{73}/total Rab10, and pLRRK2-Ser^{935}/total LRRK2, normalized to the average of LRRK2 WT values. The data shown are the mean ± SD of three determinations. (**C**) Cryo-EM maps of the Rab32–LRRK2 complex. (**D**) Summary of LRRK2 kinase activity and LRRK2 states observed in the cryo-EM study of LRRK2 alone, in the presence of Rab32, or in the presence of Rab29.